Journal of Radioanalytical and Nuclear Chemistry (2022) 331:985–997
https://doi.org/10.1007/s10967-021-08166-0

Investigation of modified orange peel in the removal of Cd^{2+}, Co^{2+} and Zn^{2+} from wastewater

Sara S. Mahrous[1] · E. A. Abdel Galil[1] · Muhammad S. Mansy[2,3]

Received: 29 September 2021 / Accepted: 11 December 2021 / Published online: 15 January 2022

Abstract
Eco-friendly and cost-effective adsorbent material was successfully synthesized from orange peel (OP). Using H_2O_2, the modification of the prepared OP was carried out. SEM, XRD, EDX, TGA and FTIR analysis was conducted to characterize the modified orange peel (MOP). MOP was tested to remove (Cd^{2+}, Co^{2+} and Zn^{2+}) metal ions from wastewater. From the results, the sorption reaction kinetics follows pseudo-second-order. It also observed that the sorption process was more fitted to the Freundlich isotherm model. It was found that Q_{max} values were equal to (46.25, 19.21 and 7.43) $mg.g^{-1}$ for Cd^{2+}, Co^{2+} and Zn^{2+}, respectively.

Keywords Orange peel · Cadmium · Cobalt · Zinc · Wastewater

Introduction

Environmental pollution caused by the regular release of industrial waste effluents into terrestrial and water has become a boundless problem, particularly in the twenty-first century. This is due to the presence of various pollutants in these aqueous wastes, which could have a negative impact on human and animal health. Due to their non-biodegradability, toxicity and hazardous nature, zinc, cadmium and cobalt are classified as dangerous to health once they enter the human body through the food chain. As a result, different legal implementations are necessary to minimize heavy metals and materials contaminated with radioactive elements consumption from various ecological samples based on pollution levels and locations. Ion exchange, flotation and adsorption are the most dominant techniques for liquid waste treatment. Adsorption is considered the most feasible and cost-effective method for removing metal ions from aqueous solutions. This is due to the development of low-cost adsorbents and adsorbent precursors, including the simplicity of handling and functionality [1].

Different organic and inorganic sorbent materials were investigated to remove metal ions from radioactive and non-radioactive wastewater. El-Din et al. [2] used Nano-sized Prussian blue to remove ^{137}Cs. Mansy et al. [3] used aluminium silicate modified with magnesia to remove ^{60}Co, ^{137}Cs, and $^{152+154}Eu$ from radioactive wastewater. Abdel-Galil et al. [4] investigated the removal of ^{60}Co, ^{137}Cs and ^{140}La from radioactive wastewater using cellulose modified by HO_7Sb_3. Recently, Hai et al. [5] studied the applicability of multiwall carbon nanotubes to remove Cd^{2+}. Several studies were conducted on the orange peel as a sorbent material but in activated carbon or biochar forms [6, 7].

In the present work, a feasibility study was conducted to evaluate the Biosorbent orange peel as a raw material modified only with H_2O_2 without conversion into activated carbon to remove Cd^{2+}, Co^{2+}, and Zn^{2+} metal ions from wastewater. The preparation technique, along with the material characterization, was also discussed. The validation of the present work material includes both isotherm and kinetic models to understand the sorption mechanism.

✉ Sara S. Mahrous
drsaramahrous.eaea@yahoo.com

1 Environmental Radioactive Pollution Department, Hot Labs and Waste Management Center, Egyptian Atomic Energy Authority, Cairo, Egypt

2 Analytical Chemistry Department, Hot Labs and Waste Management Center, Egyptian Atomic Energy Authority, Cairo, Egypt

3 Radioactive Waste Management Unit, Hot Labs and Waste Management Center, Egyptian Atomic Energy Authority, Cairo, Egypt

Experimental

NaOH, ethanol, and H_2O_2 are manufactured by Sigma-Aldrich and used without further purification.

Preparation and modification of orange peel

Orange peel waste was collected from the Egyptian juice markets. The orange peel was first washed with water, then cut into small pieces, dried in the daylight for one day, and then put in the oven at 50 °C for another day. OP was crushed using a crushing mill. The powdered material was soaked in NaOH (1%) and ethanol for 24 h. The solution was filtered and dried at 50 °C. The OP surface modification was carried out as the following; about 40 g of powdered material was added to 500 mL of 50% H_2O_2 solution and stirred at 25 °C for 48 h. Finally, the precipitate was washed several times with distilled water and kept in the oven to dry at 50 °C for another day. A schematic diagram describes the preparation and modification of OP is presented in Fig. 1.

Characterization of orange peel

Several characterizations of the prepared OP and modified one were carried out. The scanning electron microscope, SEM (JEOL-JSM-6510LA, Tokyo, Japan), was used to study the surface morphology. Crystal structure, particle size, and phase were investigated using X-ray diffraction XRD (Shimadzu XD-D1, Japan) equipped with Cu-k_α target. Elemental analysis was carried out using the energy dispersive X-Ray analysis EDX model (JSM-5600 LV, JEOL, Japan), equipped with an Oxford Inca EDX detector for compositional analysis. The thermal stability of the MOP was tested via a thermo-gravimetric analysis TGA test (Shimadzu DTG-60/60H-Thermal Analyzer, Japan). Finally, the active function groups were identified using Fourier transform infrared spectroscopy FT-IR analysis (FT-IR, Nicolet spectrometer, Meslo, USA).

Adsorption experiments

The batch experiments were conducted to evaluate the applicability of the MOP to adsorb Cd^{2+}, Co^{2+}, and Zn^{2+} species from wastewater. Experiments were conducted in 15 ml glass bottles with 50 mg powdered MOP and 5 ml of the specified cation species solution. The glass bottles were sealed and placed on a thermostatic shaker, set to 250 rpm for the studies; 298 ± 1 K has been set as the room temperature. An appropriate amount of 0.1 M HCl or NH_4OH was added to adjust the pH. Double distilled water was used to prepare the solutions for the experiment.

Experiments with solution concentrations ranging from 50 to 500 mg. L^{-1} were used to examine the effect of initial adsorbate concentration. Also, a contact time from 10 to 300 min under the optimum conditions, were investigated.

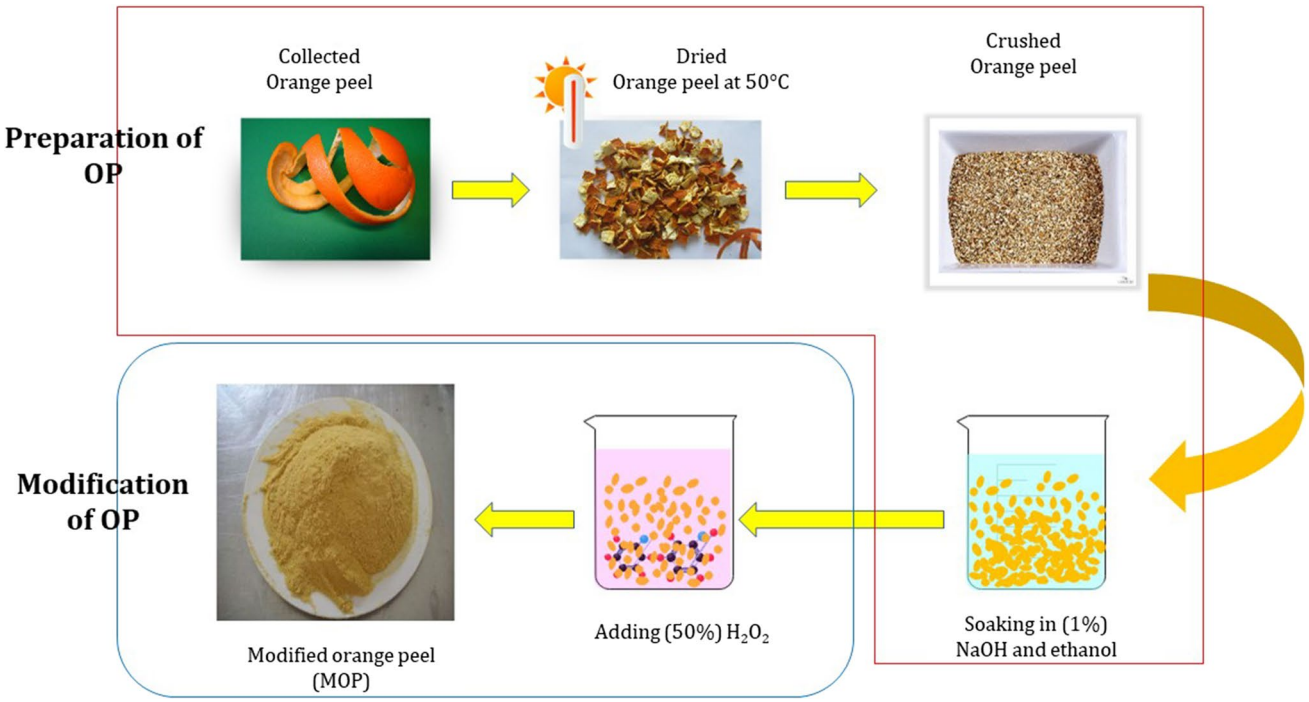

Fig. 1 Graphical abstract for preparation and modification of OP

The removal efficiency (%R) was calculated as:

$$\%R = \frac{(C_o - C_e)}{C_o} \times 100 \quad (1)$$

The adsorption capacities at any time (q_t) and equilibrium (q_e) can be calculated using the following equations:

$$q_e = (C_o - C_e) \times \frac{V}{m} \text{ (mg/m)} \quad (2)$$

and

$$q_t = (C_o - C_t) \times \frac{V}{m} \text{ (mg/m)} \quad (3)$$

The decontamination factor (DF) is calculated as:

$$D.F. = \frac{A_o}{A_f} \quad (4)$$

Results and discussion

Characterization

Scanning electron microscope

The microstructure and surface morphology of the prepared OP (upper images) and MOP (lower images) at different magnifications power of (50, 10 and 2) µm are shown in the SEM micrographs in Fig. 2.

Figure 2 upper images show that the OP surface morphology takes the form of well-structured layers without a well-defined direction due to pectin, cellulose, and hemicellulose forming the orange peel with a small number of porous. On the other hand, the lower section of Fig. 2 shows the surface morphology of MOP with highly heterogeneous cavities and pores. Also, after modifying the

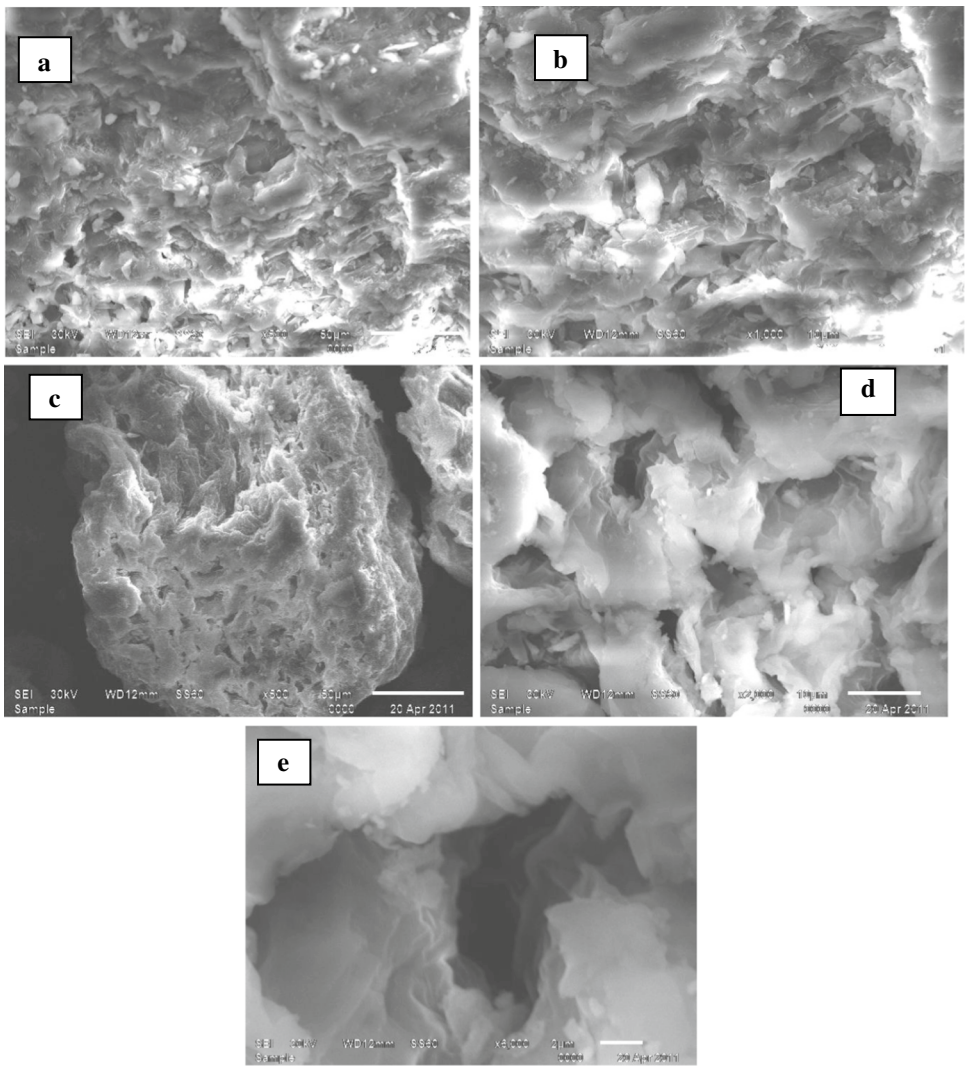

Fig. 2 SEM images a and b for the OP before modification at 50 and 10 µm, images c, d and e are for MOP at 50, 10 and 2 µm

OP surface, it can be seen that the modification process increases the active sites and cavities on the surface.

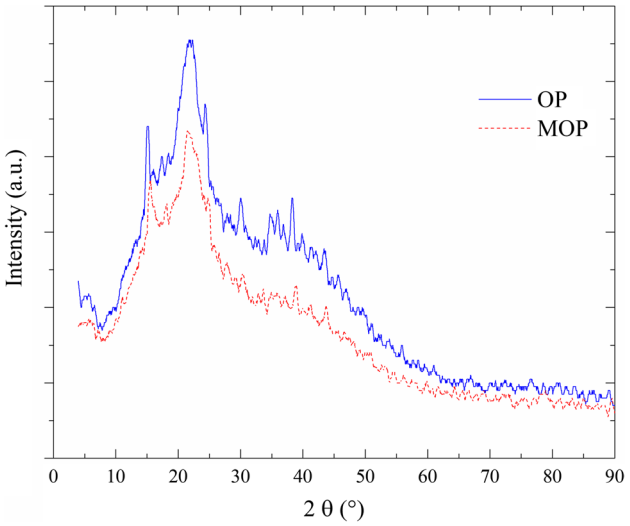

Fig. 3 XRD pattern for OP and MOP

X-ray diffraction

Figure 3 shows that the OP and MOP have an amorphous structure, expected from organic adsorbent materials. Also, the pattern shows known peaks at a 2θ value range of (15°–25°) which may be attributed to cellulose structure [8].

Elemental analysis using EDX

The OP and MOP elemental percentages are shown in Fig. 4, generated by the EDX technique and listed numerically in Table 1.

It is apparent from Table 1 and Fig. 4 that the highest concentration is attributed to carbon and oxygen, which are the main components in the natural orange peel. A negligible percent from impurities such as Na, K, Fe Ca, and S was determined and may be due to the minerals naturally on the OP.

FTIR

The FT-IR in the OP and MOP transmission spectra appear in Fig. 5. In addition, the active functional groups are listed in Table 2. The widespread extensive band absorption around 3427.44 cm^{-1} corresponding to the stretching vibration of O–H groups was due to the intra–intermolecular

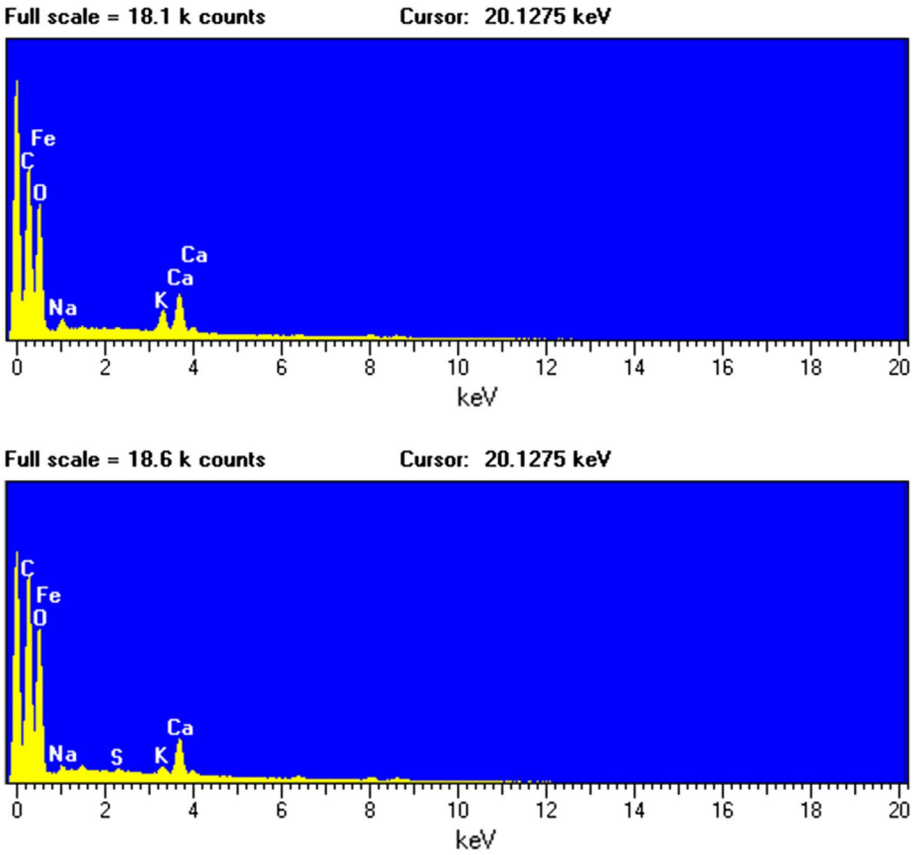

Fig. 4 EDX spectra for (OP) and (MOP) adsorbent material

Table 1 Elemental composition of orange peel (OP) and modified orange peel (MOP) adsorbent material from EDX spectra

Element	Orange peel (OP)		Modified orange peel (MOP)	
	Element (%)	Atomic (%)	Element (%)	Atomic (%)
C	35.75	44.63	38.81	47.37
O	54.63	51.21	54.49	49.94
Na	2.05	1.34	1.04	0.66
K	2.40	0.92	0.74	0.28
Ca	4.88	1.83	3.88	1.42
Fe	0.29	0.08	0.77	0.20
S	–	–	0.27	0.12

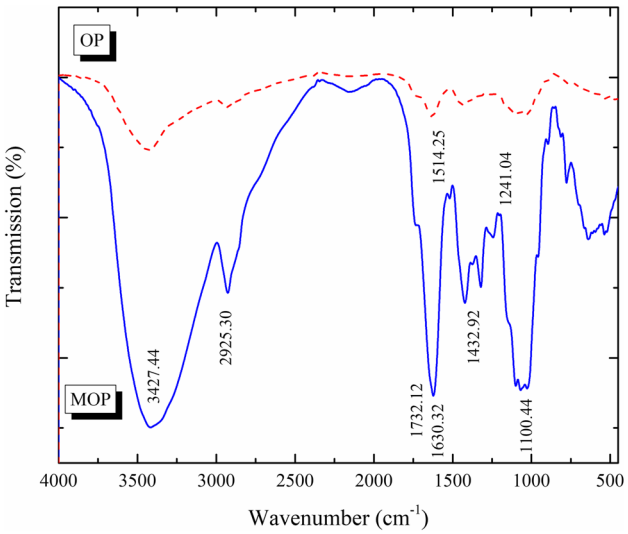

Fig. 5 FT-IR spectra for OP and MOP adsorbent material as a function of wavenumber (cm^{-1})

interactions, which occur due to carboxylic and phenolic groups [9]. The peak at 2925.30 cm^{-1} is attributed to aliphatic acids C–H stretching vibrations. The peak observed at 1732.12 cm^{-1} may be due to the stretching vibrations for C=O due to the bonds of carboxylic groups non-ionic (–COOH, $–COOCH_3$). The peaks at 1630.2 and 1514.25 cm^{-1} correspond to skeletal aromatic vibrations of C=C in lignin. The peak at 1432.92 cm^{-1} is attributed to phenol -COO- symmetric vibrations. Finally, the peak at 1100.44 cm-1 may correspond to the primary OH group in lignin or hemicellulose [10].

Thermal analysis TGA

The TGA profile of MOP is shown in Fig. 6. The MOP's TG analysis reveals five distinct regions of mass loss up to 700 °C. The first region reflects the initial mass loss due to humidity, up to 200 °C. Other mass loss regions may be associated with the degradation of hemicellulose, cellulose, and lignin, the three essential structural components of biomass. [11].

From 200 to 350 °C, a significant weight loss which was attributed to hemicellulose decomposition, well-suited with those of the values described by Zapata et al. [11], which showed that the hemicelluloses decompose at temperatures between 200 and 260 °C, producing more volatiles, fewer tars, and fewer chars than cellulose. In a temperature range of 260–360 °C, the end of hemicellulose decomposition could be seen, with cellulose degradation taking precedence. The gradual lignin degradation provides the third mass loss stage from 360 to 450 °C. Finally, the peaks between 450 °C and 700 °C are attributable to char or tar remnants [11].

Adsorption Batch experiments

Effect of the adsorbent amount

The effect of adsorbent amount on removing Cd^{2+}, Co^{2+}, and Zn^{2+} was studied, and the obtained data is shown in Fig. 7. It was evident from Fig. 7 that the removal of Cd^{2+}, Co^{2+}, and Zn^{2+} has the same behaviour as it increases by increasing the adsorbent amount until reaching saturation at the adsorbent amount beyond 0.05 g. So, the optimum adsorbent dosage achieving the highest percent removal equals 0.05 g/5 mL.

Effect of initial concentration

The effect of the initial concentration of the adsorbate was studied by performing the adsorption experiment with different initial concentrations of Cd^{2+}, Co^{2+}, and Zn^{2+}

Table 2 The identified active functional groups of OP and MOP adsorbent material

Wave number (cm^{-1})	Functional group
3427.44	-OH stretching vibrations
2925.30	C–H stretching vibrations
1732.12	C=O stretching for carboxy groups (-COOH, $-COOCH_3$)
1630.32 and 1514.25	Skeletal aromatic vibrations of C=C
1432.92	Phenol -COO- symmetric vibrations
1100.44	primary OH group in lignin or hemicellulose

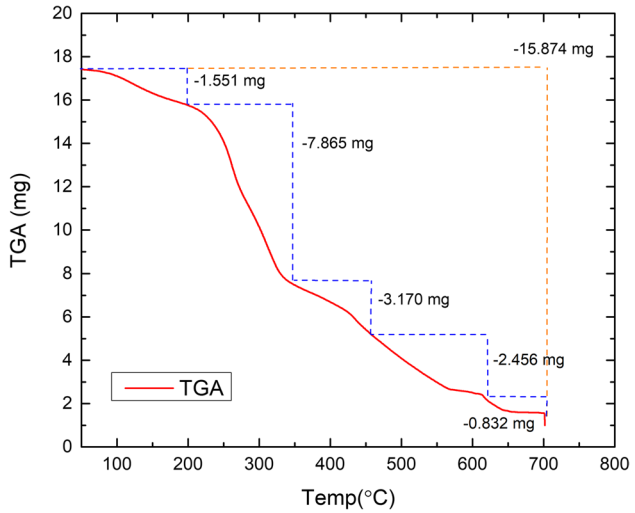

Fig. 6 TGA for the MOP adsorbent material

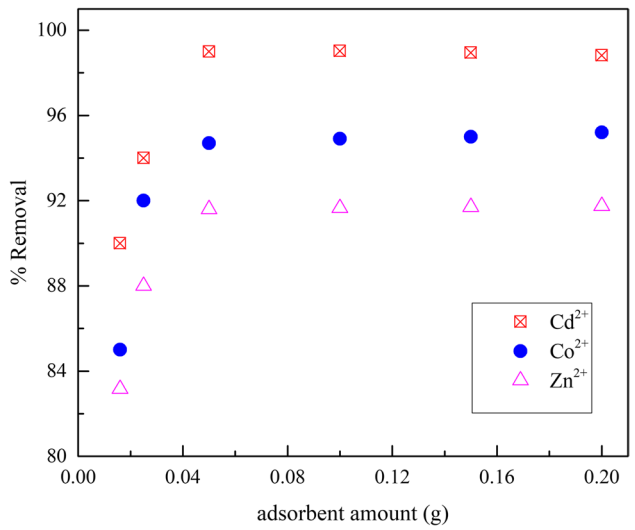

Fig. 7 The effect of adsorbent amount on Cd^{2+}, Co^{2+}, and Zn^{2+} removal by MOP

(50–500 mg .L^{-1}) until equilibrium was reached; results are displayed in Fig. 8.

The results show that the adsorption of Cd^{2+}, Co^{2+}, and Zn^{2+} was decreased with increasing initial concentration. This behaviour could be described as the total number of moles of metal ions increases with increasing the solution concentration compared to the existing adsorbent active sites.

Effect of pH

The pH value of the solution plays a significant role in the adsorption process. Therefore, the adsorption experiments were carried out at various pH values 1–6, and the result is

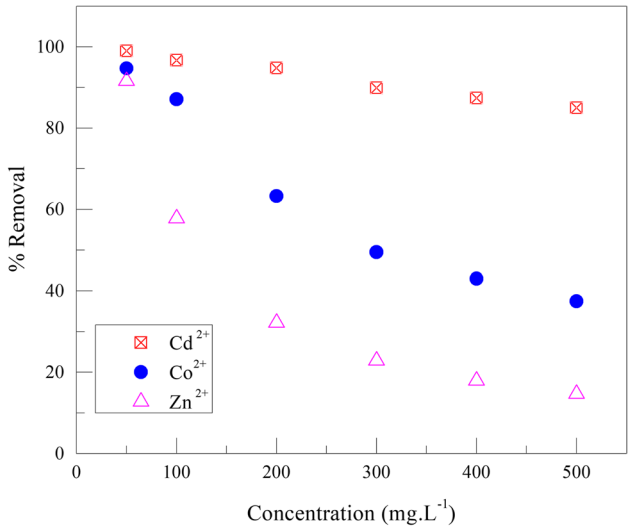

Fig. 8 The effect of concentration of Cd^{2+}, Co^{2+}, and Zn^{2+} removal by MOP

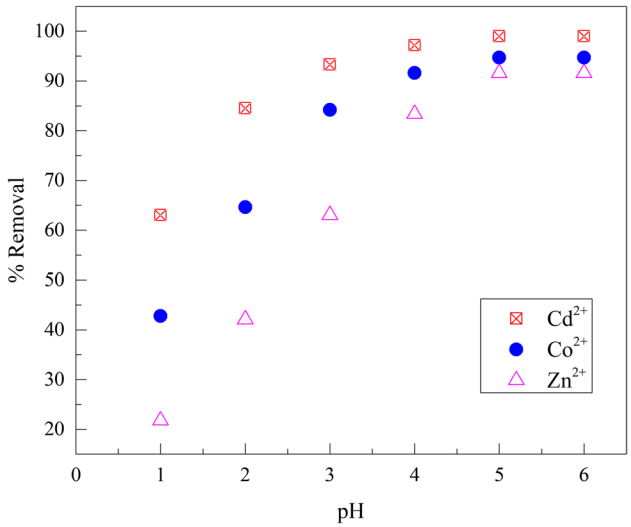

Fig. 9 The effect of solution pH on removing Cd^{2+}, Co^{2+}, and Zn^{2+} by MOP

presented in Fig. 9. It is apparent that, during the pH variation, the adsorption efficiency rapidly increased at pH values from 1 up to 3. After that, the adsorption efficiency increase is slow until reaching saturation at a pH value of 5. Therefore, pH = 5 was taken as the optimum, at which the maximum adsorption efficiency was achieved.

Effect of contact time

The effect of contact time on the adsorption process was studied by performing the adsorption experiment with an initial concentration of 50 mg .L^{-1} at different contact times ranging from (10–300) min. Data plotted in Fig. 10 shows

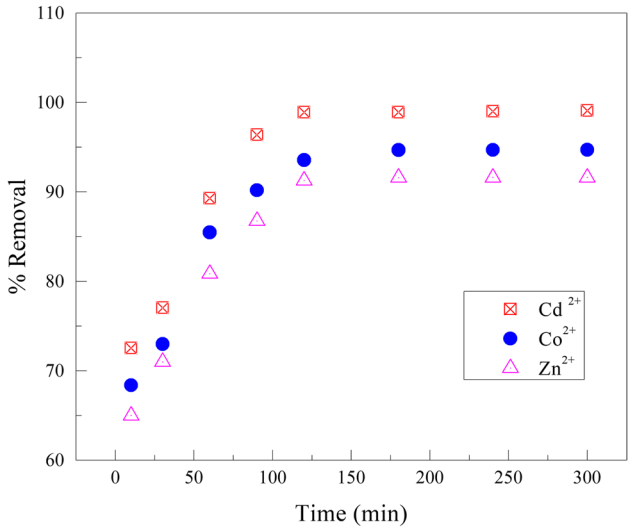

Fig. 10 The effect of contact time in removing Cd^{2+}, Co^{2+}, and $Zn^{2+}$by MOP

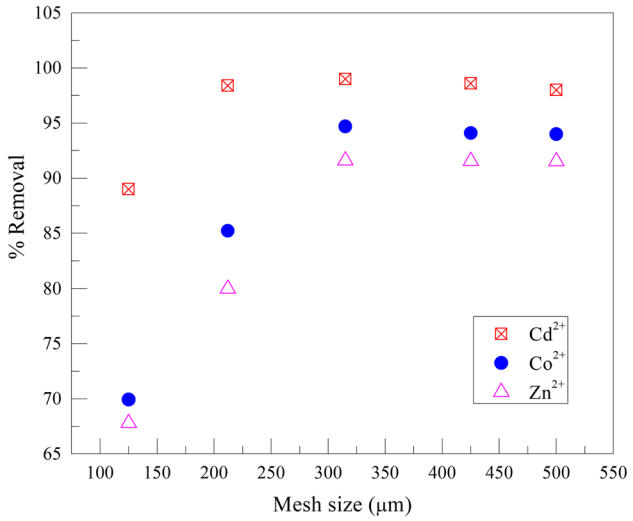

Fig. 11 The effect of adsorbent mesh size in removing Cd^{2+}, Co^{2+}, and Zn^{2+} by MOP

that the adsorption efficiency of Cd^{2+}, Co^{2+}, and Zn^{2+} onto the MOP increased with contact time increasing. However, a slight decrease in the adsorption was noticed when the contact time reached equilibrium. The equilibrium time was found to be 120 min for all studied cations.

Effect of adsorbent mesh size

The effect of adsorbent mesh size on the adsorption process was studied by performing the adsorption experiments at different adsorbent mesh sizes of (125–500) μm. The results from the adsorption experiments are plotted in Fig. 11.

Figure 11 shows that the %removal of Cd^{2+}, Co^{2+}, and Zn^{2+} adsorbed by MOP was increased by increasing the mesh size till reaching its maximum value at 315 μm.

Effect of competing ions

To simulate the influence of real water body on adsorption process, the effect of competing ions such as (Na^{+}, Mg^{2+}, and Ca^{2+}) at concentrations of (5,10,15 and 20) mg $.L^{-1}$ was carried out with a concentration of 50 mg L^{-1} of Cd^{2+}, Co^{2+}, and Zn^{2+}. The experiment result is listed in Table 3 and presented graphically in Fig. 12.

It is apparent from Table 3 that, Na^{+} competing ion shows a slight decrement in the % removal than Mg^{2+} and Ca^{2+}. This result may be due to the lower electrostatic interaction of monovalent Na^{+} than studied metal ions.

Kinetic studies of adsorption

This work tested the adsorption of Cd^{2+}, Co^{2+}, and Zn^{2+} at a temperature of 298 K with pseudo-first and Pseudo second-order kinetic models and explained the reaction mechanism involved between the functional groups in the adsorbent surface and the adsorbate metal ions.

Pseudo-first-order kinetic model

The pseudo-first-order kinetic model is stated by the following Eq. as mentioned in [12]:

$$\ln(q_e - q_t) = \ln q_t - k_1 t \tag{5}$$

where k_1 (min^{-1}) is the pseudo-first-order rate constant, q_t (mg. g^{-1}) is the amount of solute adsorbed at time t (min) and q_e (mg. g^{-1}) is the amount of solute adsorbed at saturation. The values of q_e and k_1 are calculated by plotting $\ln(q_e - q_t)$ versus t and calculate the slope and intercept, respectively. The calculation results were plotted in Fig. 13 and listed in Table 4. If the q_e obtained from experimental and theoretical are different, it indicates the insignificance of the model.

Pseudo-second-order kinetic model

The pseudo-second-order kinetic model is calculated from the following equation as mentioned by Ho and McKay [13]:

$$\frac{t}{q_t} = \frac{1}{k_2 q_e^2} + \frac{t}{q_e} \tag{6}$$

where k_2 (g. mg^{-1}. min^{-1}) is the rate constant for pseudo-second-order and q_e(mg. g^{-1}) is the amount adsorbed at equilibrium. The plot of (t/q_t) ersus t is linear and sued for calculating the pseudo-second-order rate constant. The

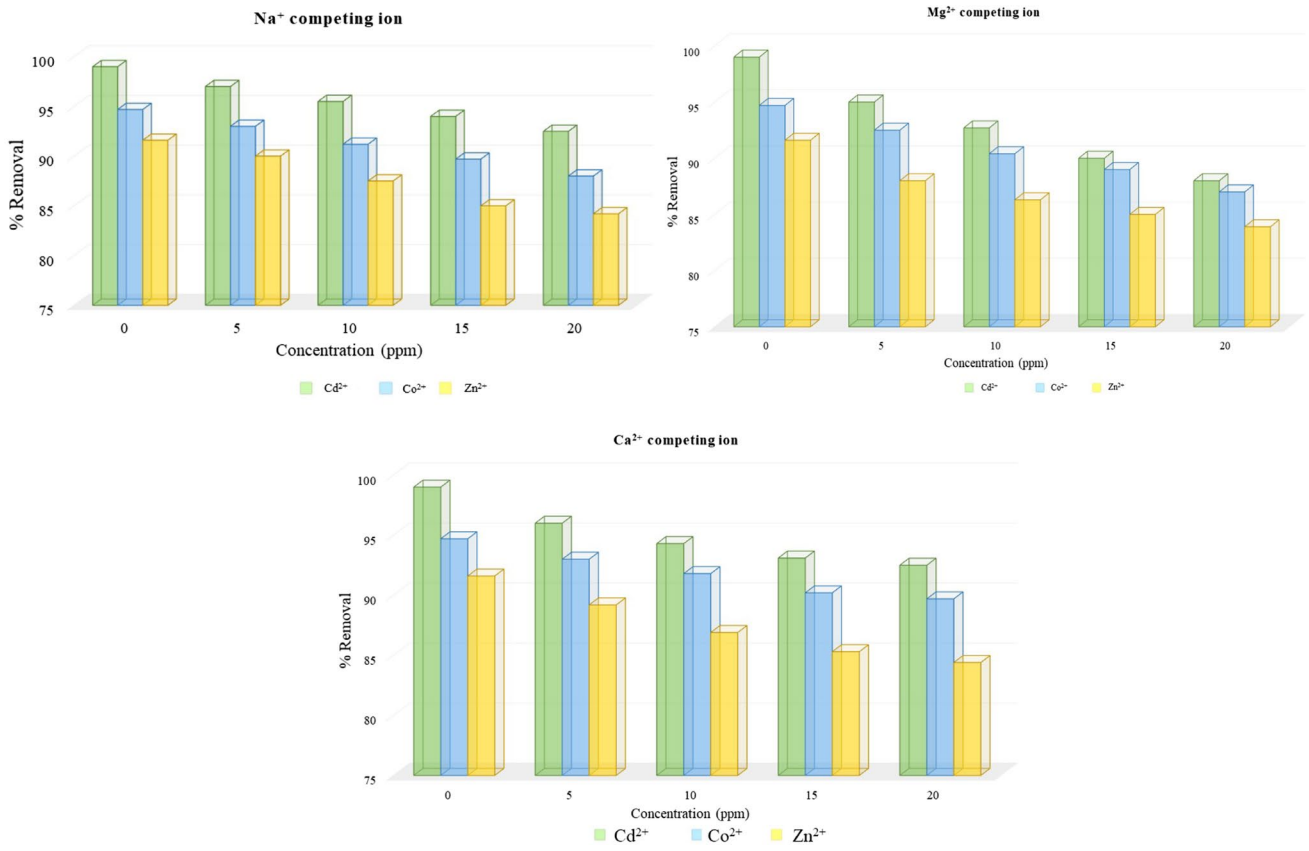

Fig. 12 The effect of competing ions on the adsorption of Cd^{2+}, Co^{2+}, and Zn^{2+} by MOP

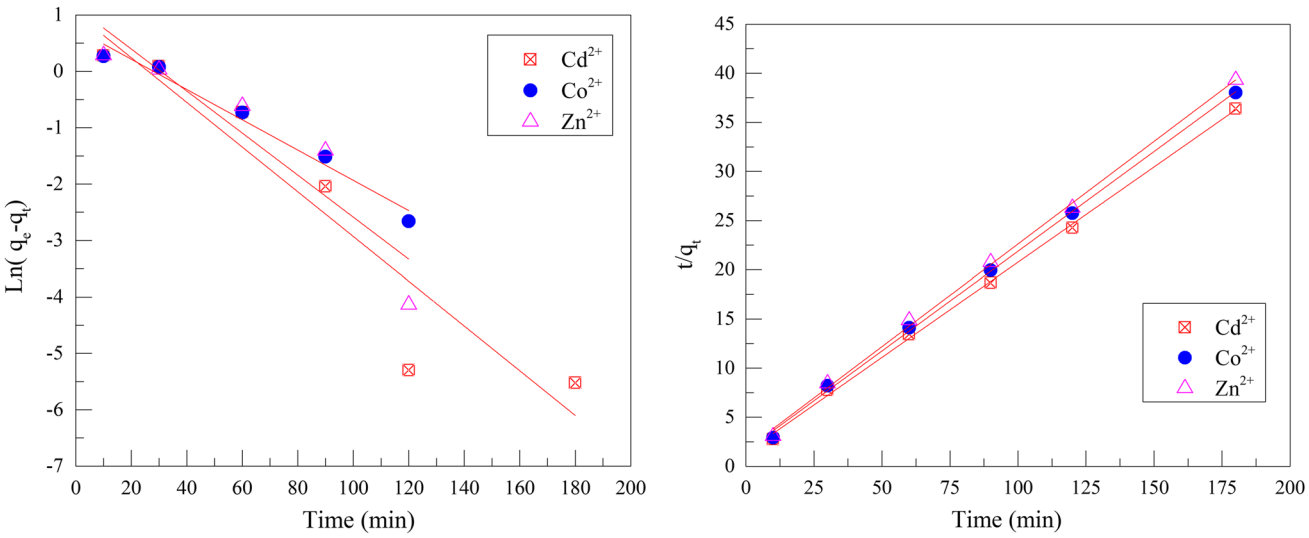

Fig. 13 Pseudo first and second-order kinetic models

kinetics adsorption behaviour of Cd^{2+}, Co^{2+}, and Zn^{2+} was represented in Fig. 13 and listed in Table 4. Concerning the data in Table 4, it is evident that the pseudo-second-order model is well fitted ($R^2 > 0.997$) with the experimental data than the first-order model ($R^2 < 0.968$). It is also noticed that q_e values from both theoretical and experimental are in the same range with slight deviation promoting the applicability of Pseudo second-order than the first-order.

Table 3 Effect of competing ions with different concentrations on the % removal of Cd^{2+}, Co^{2+}, and Zn^{2+} at pH 5.0

Cation	% Removal in the presence of Na^+, Mg^{2+} and Ca^{2+}											
	0	Na^+ concentration (mg. L^{-1})				Mg^{2+} concentration (mg. L^{-1})				Ca^{2+} concentration (mg. L^{-1})			
		5	10	15	20	5	10	15	20	5	10	15	20
Cd^{2+}	99.0	97.0	95.5	94.0	92.5	95.0	92.7	90.0	88.0	96.0	94.3	93.1	92.5
Co^{2+}	94.7	93.0	91.2	89.7	88.0	92.5	90.4	89.3	87.5	93.0	91.8	90.2	89.7
Zn^{2+}	91.6	90.0	87.5	85.0	84.2	88.0	86.3	85.0	83.9	89.2	86.9	85.3	84.4

Table 4 Comparison between the experimental and calculated q_e values of both the first and second-order adsorption kinetics at a temperature of 298 K for Cd^{2+}, Co^{2+}, and Zn^{2+} concentration of 50 mg. L^{-1} and pH 5.0

Cation	Temperature (K)	q_e exp. (mg. g^{-1})	Kinetic model					
			Pseudo first order			Pseudo second order		
			k_1 (min^{-1})	q_e cal. (mg. g^{-1})	R^2	k_2 (g .mg^{-1} . min^{-1})	q_e cal. (mg. g^{-1})	R^2
Cd^{2+}	298	4.95	0.0396	2.80	0.887	0.023	5.18	0.998
Co^{2+}	298	4.73	0.0260	2.12	0.968	0.026	4.93	0.998
Zn^{2+}	298	4.58	0.0370	3.12	0.815	0.024	4.80	0.997

Isotherm studies of adsorption

The Langmuir, Freundlich, and Dubinin–Redushkevich models were investigated in the present study to fit the experimental data and find the relation between equilibrium concentration between adsorbent and adsorbate.

Langmuir isotherm model

The Langmuir isotherm model assumes that mono-layer adsorption occurred on homogeneous surfaces, and it can be expressed by the following equation mentioned in [14]:

$$\frac{C_e}{q_e} = \frac{C_e}{Q} + \frac{1}{bQ} \tag{7}$$

where C_e (mg. L^{-1}) is the equilibrium concentration of adsorbate solution, q_e(mg. g^{-1}) is the adsorption capacity of the sample, b (L. mg^{-1}) is the adsorption coefficient, and Q (mg .g^{-1}) is the mono-layer adsorptive capacity. Experimental data for Cd^{2+}, Co^{2+}, and Zn^{2+} fitted with Langmuir adsorption isotherm model is presented in Fig. 14. Data is well fitted with the Langmuir model, and the constants were derived from the slope and intercept listed in Table 5.

Freundlich isotherm model

The Freundlich isotherm model is commonly used to find the adsorption intensity of adsorbate surfaces with non-uniform energy distribution. The linear form of the Freundlich equation is given in [15] as:

$$\log(q_e) = \log K_f + \frac{1}{n} \log C_e \tag{8}$$

where q_e (mg. g^{-1}) is the amount adsorbed at equilibrium, C_e (mg. L^{-1})is the equilibrium concentration of the adsorbate metal ions, and (K_f and n) are Freundlich constants related to the adsorption capacity and adsorption intensity, respectively. A plot of $\log(q_e)$ against $\log C_e$ is presented in Fig. 14 as straight lines with a slope $\frac{1}{n}$ and an intercept K_f. The K_f values were used to determine the adsorption capacities of the adsorbent. Table 5 shows that 1/n values were less than one; it indicates that the MOP has a heterogeneous surface nature and is favourable for the multilayer process's adsorption [7]. These results confirm that the MOP is a potential candidate for the adsorption of selected cations Cd^{2+}, Co^{2+}, and Zn^{2+}.

Table 5 concluded that the experimental data fit the Freundlich isotherm model more than the Langmuir isotherm model. These results show that the MOP has a heterogeneous surface nature. Also, the results show that both Freundlich and Langmuir are fitted well, but the Freundlich isotherm model is more dominant for the present work MOP.

Dubinin–Radushkevich isotherm model

Dubinin–Radushkevich isotherm is used to determine whether the adsorption occurred by a physical or chemical

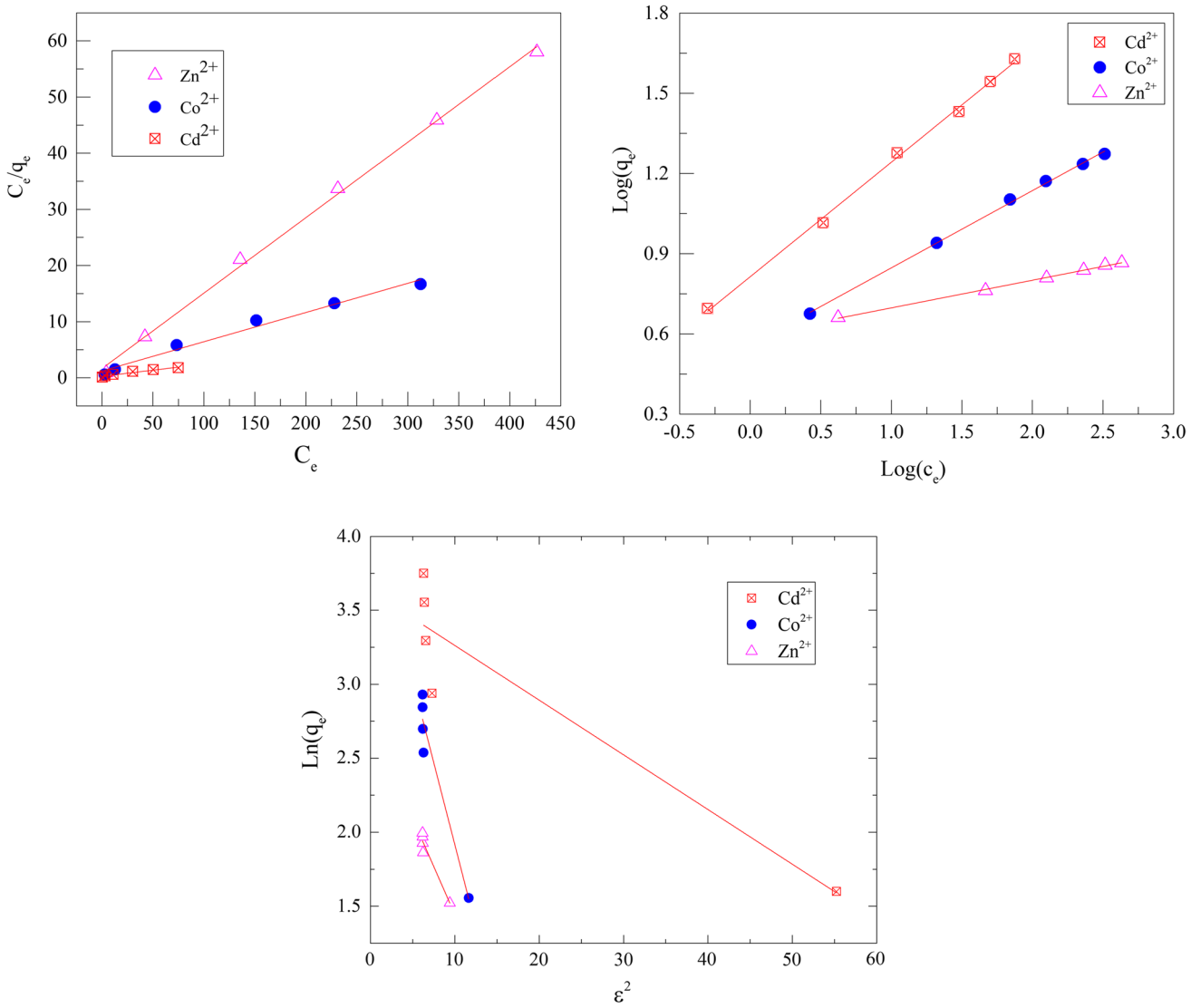

Fig. 14 Langmuir, Freundlich and D–R isotherm models

process. The linearized form of this isotherm is given as the following equation:

$$\ln q_e = \ln \chi'_m - \beta\varepsilon^2 \quad \text{and} \quad \varepsilon = RT \ln\left(1 + \frac{1}{C_e}\right) \tag{9}$$

where, q_e is the amount of ions sorbed per gram of sorbent (mg .g^{-1}), (χ'_m) is the adsorption capacity of the sorbent (mg .g^{-1}), (C_e) is the equilibrium metal ions concentration in solution, (β) adsorption energy constant (kJ^2 .mol^{-2}), (R) is the gas constant (kJ .K^{-1} .mol^{-1}) and (T) is the temperature in (K). A data plot between $\ln q_e$ and ε^2 at constant temperature was used to determine both χ'_m and β. The mean sorption energy (E) is the free energy transfer of one mole of solute from infinity to the surface of the adsorbent and was calculated as:

$$E = (-2\beta)^{-1/2} \tag{10}$$

According to the E value obtained from Dubinin–Radushkevich isotherm model, the type of interactions during the adsorption process is determined. The data obtained from the Dubinin–Radushkevich isotherm model were given in Fig. 14 and shown in Table 5.

Generally, the values of free energy change (E) can be:

- in the range of (1–8) kJ .mol^{-1}, the adsorption process is physical,
- in the range of (8–16) kJ .mol^{-1}, the adsorption process is defined by an ion-exchange mechanism,
- greater than 16 kJ .mol^{-1}, the adsorption process is chemical [3].

Table 5 Langmuir, Freundlich and D–R adsorption isotherm of Cd^{2+}, Co^{2+}, and Zn^{2+} adsorption on MOP for 298 K and initial concentration of 50 mg L^{-1} and pH 5.0

Cation	Temperature (K)	Isotherm model									
		Langmuir			Freundlich			Dubinin–Radushkevich			
		Q_{max} (mg. g^{-1})¥	b (L .mg^{-1})	R^2	1/n	k_f (mg .g^{-1})	R^2	χ'_m (mg. g^{-1})	β (kJ^2 .mol^{-2})	E (kJ .mol^{-1})	R^2
Cd^{2+}	298	46.25	0.077	0.941	0.42	6.50	0.997	30.88	0.034	3.67	0.846
Co^{2+}	298	19.21	0.042	0.980	0.28	3.54	0.998	57.39	0.219	1.50	0.917
Zn^{2+}	298	7.43	0.083	0.997	0.10	3.92	0.998	14.43	0.123	1.96	0.921

¥Saturation capacity

Table 6 Comparison of Q_{max} of MOP and other sorbent materials

Sorbent material	Maximum sorption capacity Q_{max} (mg .g^{-1})			Reference
	Cd^{2+}	Co^{2+}	Zn^{2+}	
Chitosan grafted with maleic acid	–	2.78	–	[16]
Activated bentonite	–	7.3	–	[17]
Cellulose / HO_7Sb_3	–	21.2	–	[18]
Kaolinite	–	11.0	4.9	[19]
Bagasse fly ash modified with H_2O_2	–	–	2.34	[20]
Polyelectrolyte-Coated Industrial Waste Fly Ash	6.4	–	–	[21]
Sawdust-oak modified with formaldehyde	–	–	6.1	[22]
Sawdust-black locust modified with NaOH	–	–	6.7	[22]
MWCNT-MnO_2	41.6	–	–	[5]
SWCNT-COOH	55.89	–	–	[23]
MOP	46.25	19.21	7.43	Present work

In the present work, the obtained E values for Cd^{2+}, Co^{2+}, and Zn^{2+} were 3.83, 1.51 and 2.01 kJ. mol^{-1}, respectively, indicating that physical adsorption was involved in the adsorption process.

Table 6 shows a comparison between the Q_{max} value for different organic sorbent materials for the removal of Cd^{2+}, Co^{2+}, and Zn^{2+} from wastewater.

It can be seen from Table 6 that present work, MOP has a relatively high maximum sorption capacity compared to other sorbent materials. From this result, MOP can be used successfully as a promising material for retaining Cd^{2+}, Co^{2+}, and Zn^{2+} from wastewater solutions.

Application

The evaluation of the MOP in the removal of specific radionuclides was carried out using a low-level liquid radioactive waste sample. The sample characterisation was conducted using coaxial HPGe (GEM-series, ORTEC, USA) connected to a multichannel analyzer system (MCA, Inspector 2000 Series, Canberra, USA) for 30 min. The characterization result is that the sample contains ^{137}Cs and ^{60}Co with radioactivity levels of 2000 ± 44.72 and 1700 ± 41.23 Bq.L^{-1}., respectively. Using 0.05 g MOP in a 5 mL radioactive waste sample and then shaking at 250 rpm for 120 min. After that, the solution was filtered and then counted for 30 min to find the sample's

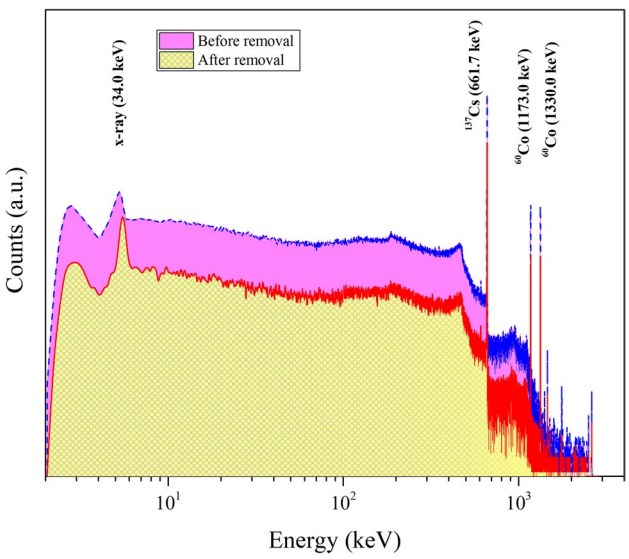

Fig. 15 Gamma spectra of a radioactive waste sample before and after decontamination measured using HPGe detector

Table 7 Radioactivity levels of initial and final counting of the waste sample along with the decontamination factor and %eff

Radionuclides	Initial activity ($Bq.L^{-1}$)	Final activity ($Bq.L^{-1}$)	D.F.	% eff
^{60}Co	2000 ± 44.72	92 ± 9.59	21.74	95.4
^{137}Cs	1700 ± 41.23	224 ± 14.9	7.58	86.8

final radioactivity level. The result of counting the initial and final waste sample is plotted in Fig. 15, and the data obtained are listed in Table 7.

It is evident from Table 7 that MOP is proficient in removing both ^{137}Cs and ^{60}Co from liquid radioactive waste samples by %eff. of 86.8 and 95.4, respectively, confirming the batch experiment results for Co metal ions. In addition, the decontamination factor reaches 21.74 in the case of ^{60}Co and 7.58 for ^{137}Cs.

Conclusion

Modified orange peel showed promising results in removing Cd^{2+}, Co^{2+}, and Zn^{2+} metal ions from wastewater. It also showed that MOP has a suitable adsorption capacity for Cd^{2+} (46.25 $mg.g^{-1}$), Co^{2+} (19.21 $mg.g^{-1}$), and Zn^{2+} (7.43 $mg.g^{-1}$). The batch experiments found that the optimum adsorption equilibrium time was about 120 min at 298 K and pH 5 for all studied metal ions. The experimental results were analysed using the Langmuir and Freundlich models, and it was found that the sorption process is more fitted to the Freundlich equation than the Langmuir. The obtained E value from the D–R model is below eight kJ. mol^{-1} for Cd^{2+}, Co^{2+}, and Zn^{2+} metal ions; it suggests that the sorption process is physical. The data indicate that each metal ion's adsorption kinetics on the MOP follow the pseudo-second-order rate expression. Finally, MOP is a proficient sorbent material for removing both ^{137}Cs and ^{60}Co from low-level-liquid radioactive waste samples by % eff. of 86.8 and 95.4, respectively, with high D.F. values.

Declarations

Conflict of interst Sara S. Mahrous, E.A. Abdel-Galil and Muhammad S. Mansy certify that they have NO affiliations with or involvement in any organization or entity with any financial interest (such as honoraria; educational grants; participation in speakers' bureaus; membership, employment, consultancies, stock ownership, or other equity interest; and expert testimony or patent-licensing arrangements), or non-financial interest (such as personal or professional relationships, affiliations, knowledge or beliefs) in the subject matter or materials discussed in this manuscript and report the following details of affiliation or involvement in an organization or entity with a financial or non-financial interest in the subject matter or materials discussed in this manuscript.

References

1. Olatunji MA, Khandaker MU, Amin YM, Mahmud HNME (2016) Cadmium-109 radioisotope adsorption onto polypyrrole coated sawdust of dryobalanops aromatic: kinetics and adsorption isotherms modelling. PLoS ONE 11:e0164119. https://doi.org/10.1371/JOURNAL.PONE.0164119
2. El-Din AMS, Monir T (2019) Sayed MA (2019) Nano-sized Prussian blue immobilized costless agro-industrial waste for the removal of cesium-137 ions. Environ Sci Pollut Res 2625(26):25550–25563. https://doi.org/10.1007/S11356-019-05851-2
3. Mansy MS, Hassan RS, Selim YT, Kenawy SH (2017) Evaluation of synthetic aluminum silicate modified by magnesia for the removal of 137Cs, 60Co and 152+154Eu from low-level radioactive waste. Appl Radiat Isot 130:198–205. https://doi.org/10.1016/j.apradiso.2017.09.042
4. Abdel-Galil EA, Moloukhia H, Abdel-Khalik M, Mahrous SS (2018) Synthesis and physico-chemical characterization of cellulose/HO7Sb3 nanocomposite as adsorbent for the removal of some radionuclides from aqueous solutions. Appl Radiat Isot 140:363–373. https://doi.org/10.1016/J.APRADISO.2018.07.022
5. Hai T, Hung L, Phuong T et al (2019) Multiwall carbon nanotube modified by antimony oxide (Sb2O3/MWCNTs) paste electrode for the simultaneous electrochemical detection of cadmium and lead ions. Microchem J 153:104456. https://doi.org/10.1016/j.microc.2019.104456
6. Bediako JK, Lin S, Sarkar AK et al (2020) Evaluation of orange peel-derived activated carbons for treatment of dye-contaminated wastewater tailings. Environ Sci Pollut Res 27:1053–1068. https://doi.org/10.1007/s11356-019-07031-8
7. Pandiarajan A, Kamaraj R, Vasudevan S, Vasudevan S (2018) OPAC (orange peel activated carbon) derived from waste orange peel for the adsorption of chlorophenoxyacetic acid herbicides from water: adsorption isotherm, kinetic modelling and thermodynamic studies. Bioresour Technol 261:329–341. https://doi.org/10.1016/j.biortech.2018.04.005
8. Akinhanmi TF, Ofudje EA, Adeogun AI et al (2020) Orange peel as low-cost adsorbent in the elimination of Cd(II) ion: kinetics, isotherm, thermodynamic and optimization evaluations. Bioresour Bioprocess 7:34. https://doi.org/10.1186/s40643-020-00320-y
9. Santos CM, Dweck J, Viotto RS et al (2015) Application of orange peel waste in the production of solid biofuels and biosorbents. Bioresour Technol 196:469–479. https://doi.org/10.1016/j.biortech.2015.07.114
10. Yang H, Yan R, Chen H et al (2007) Characteristics of hemicellulose, cellulose and lignin pyrolysis. Fuel 86:1781–1788. https://doi.org/10.1016/J.FUEL.2006.12.013
11. Zapata B, Balmaseda J, Fregoso-Israel E, Torres-García E (2009) Thermo-kinetics study of orange peel in air. J Therm Anal Calorim 98:309. https://doi.org/10.1007/s10973-009-0146-9
12. Lagergren S (1907) Zur Theorie der sogenannten Adsorption gelöster Stoffe. Zeitschrift für Chemie und Ind der Kolloide 2:15–15. https://doi.org/10.1007/BF01501332

13. Ho YS, Mckay G (1999) Pseudo-second order model for sorption processes
14. Langmuir I (1917) The constitution and fundamental properties of solids and liquids. II. Liquids. [1]. J Am Chem Soc 39:1848–1906. https://doi.org/10.1021/ja02254a006
15. Freundlich HM (1906) Over the adsorption in solution. Phys Chem A 57:385–470
16. Yin Y, Wang J (2017) Removal of cobalt ions from aqueous solution using chitosan grafted with maleic acid by gamma radiation. Nucl Eng Technol. https://doi.org/10.1016/j.net.2017.11.007
17. Al-Shahrani SS (2014) Treatment of wastewater contaminated with cobalt using Saudi activated bentonite. Alexandria Eng J 53:205–211. https://doi.org/10.1016/J.AEJ.2013.10.006
18. Mahrous S, Abdel-Galil E, Belacy N, Saad E (2019) Adsorption behavior and practical separation of some radionuclides using cellulose/HO7Sb3. Desalin Water Treat 152:124–132
19. Yavuz Ö, Altunkaynak Y, Güzel F (2003) Removal of copper, nickel, cobalt and manganese from aqueous solution by kaolinite. Water Res 37:948–952. https://doi.org/10.1016/S0043-1354(02)00409-8
20. Gupta VK, Jain R, Mittal A et al (2012) Photo-catalytic degradation of toxic dye amaranth on TiO2/UV in aqueous suspensions. Mater Sci Eng C 32:12–17
21. Olabemiwo FA, Tawabini BS, Patel F et al (2017) Cadmium removal from contaminated water using polyelectrolyte-coated industrial waste fly ash. Bioinorg Chem Appl 2017:7298351. https://doi.org/10.1155/2017/7298351
22. Zwain HM, Vakili M, Dahlan I (2014) Waste material adsorbents for zinc removal from wastewater: a comprehensive review. Int J Chem Eng 2014:347912. https://doi.org/10.1155/2014/347912
23. Sahu MK, Mandal S, Yadav LS et al (2016) Equilibrium and kinetic studies of Cd(II) ion adsorption from aqueous solution by activated red mud. Desalin Water Treat 57:14251–14265